

## Fast Prediction of Thermal History in Large-Scale Parts Fabricated Via a Laser Metal Deposition Process

Lei Yan<sup>1,4</sup>, Tan Pan<sup>1</sup>, Joseph W. Newkirk<sup>2</sup>, Frank Liou<sup>1</sup>, Eric E. Thomas<sup>3</sup>, Andrew H. Baker<sup>3</sup>,  
James B. Castle<sup>3</sup>

<sup>1</sup>Department of Mechanical and Aerospace Engineering

<sup>2</sup>Department of Materials Science and Engineering

Missouri University of Science and Technology, Rolla, MO, USA

<sup>3</sup>The Boeing Company, St. Louis, MO

<sup>4</sup>Email: lyvh8@mst.edu, lei.aaron.yan@gmail.com

### Abstract

Laser metal deposition (LMD) has become a popular choice for the fabrication of near-net shape complex parts. Plastic deformation and residual stresses are common phenomena that are generated from the intrinsic large thermal gradients and high cooling rates in the process. Finite element analysis (FEA) is often used to predict the transient thermal cycle and optimize processing parameters; however, the process of predicting the thermal history in the LMD process with the FEA method is usually time-consuming, especially for large-scale parts. Herein, multiple 3D FEA models with simple assumptions on the heat source and its loading methods are compared and validated with experimental thermocouple data.

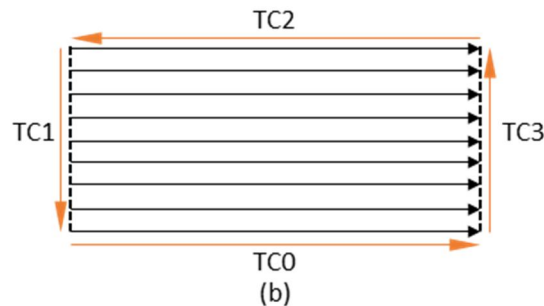
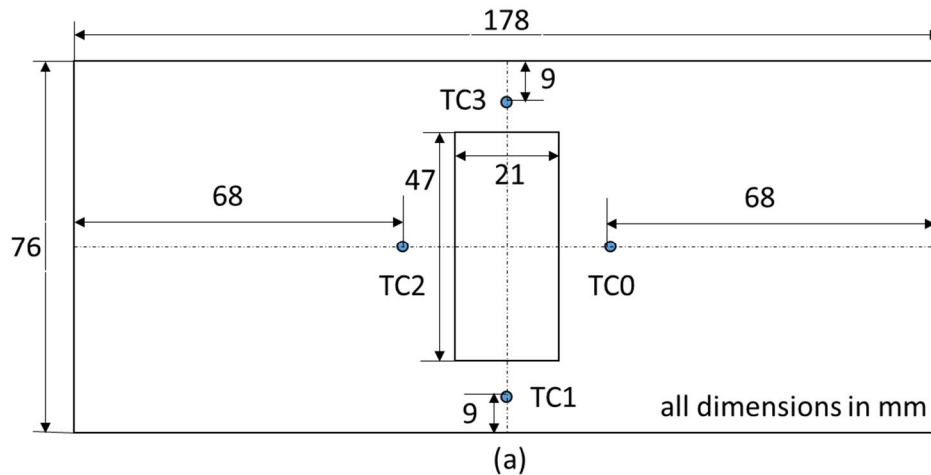
### Introduction

In the laser metal deposition (LMD) process, a description of the transient temperature fields is important for subsequent analyses such as microstructure evolution, residual stress, and distortion. Many efforts have been put on the temperature field analysis and are mainly based on the finite element analysis (FEA) method [1-5]. In literature, a commonly used method to mimic the material addition process is called the “dummy material method” [3] or the “element birth and death method” [5], which use active elements in the finite element model according to a predefined deposition strategy. The aforementioned methods usually include a computational intensive model as not only do the minimum required time increments in transient heat transfer analysis need to be met [6], but also a mesh convergence needs to be achieved, which requires a minimum element size relative to the laser beam diameter [5]. When applied, the conventional methods to predict transient temperature history in a large-scale part fabrication process increase the model size tremendously. In some cases, a precise description of the thermal history in the laser deposition process is not necessary and only a fast prediction of the peak temperature will be needed for the process plan. Herein, two methods called track-heat-source and layer-heat-source are proposed for fast prediction of transient thermal history in large-scale part fabrication via the LMD process.

### Experimental Set-up and Methods

A Ti-6Al-4V block was built on a DMG-Mori Lasertec 4300 3D hybrid machine with the following processing parameters: laser power 1680 W, laser beam spot size 4 mm, powder feed

rate 29.7 g/min, and travel speed 1000 mm/min. The experimental set-up is shown in Fig. 1. Fig. 1 (a) shows the thermocouple locations on the substrate. The deposit was fabricated according to the path plan shown in Fig. 1 (b), where nine single-direction laser scans were applied and a perimeter pass was performed on every layer. To provide a flat deposition on all corner walls, the perimeter pass was doubled every other layer based on trial-and-error. Fig. 1 (c) shows the thermocouples were fixed on the substrate with high temperature thermally conductive paste and temperature was recorded with a data acquisition instrument. Two holes shown in Fig. 1 (c) were used for mounting the substrate on a base plate. The final product is shown in Fig. 1 (d). Due to the working condition differences among varies LMD systems, there is no comparison with other groups' work and only focused on the experimental data obtained from our LMD system. To quickly predict the transient thermal history of a large-scale part build on this machine, an FEA model suitable for this process was developed and the predicted temperature fields will be used for subsequent analyses such as oxidation, residual stress, and distortion in the future.



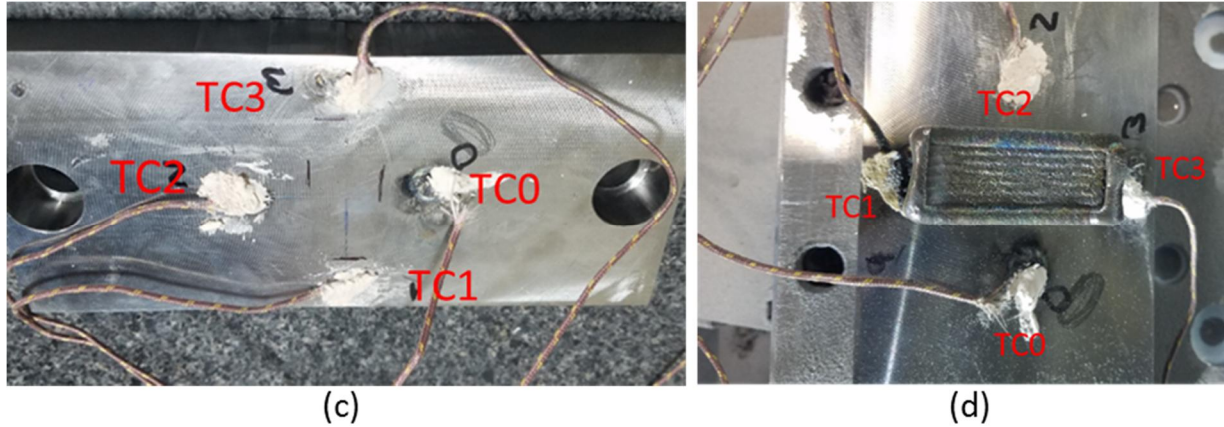


Fig. 1 Experimental set-up. (a) thermocouple locations, (b) laser scanning pattern, (c) thermocouples on the substrate before deposition, (d) final deposit.

### Modeling Procedures

In our previous work of simulating the LMD process, the heat source was modeled with a conventional method as thermal flux density ( $\text{watt}/\text{m}^2$ ) or heat generation rate ( $\text{watt}/\text{m}^3$ ) that moves place to place according to a scanning strategy [5,7], which requires a minimum element size ( $<1/6$  laser beam diameter) to meet the requirement of mesh convergence assessment. This criteria results in a large number of elements and nodes in the meshed model and results in a long simulation time. To reduce the model size and computational time, and make it feasible for fast prediction of the temperature in the LMD process, especially for large-scale parts, some assumptions and simplifications were proposed and implemented in the model:

1. In the finite element model, the thermal load in both track- and layer-heat-source scenarios are applied sequentially in the form of thermal flux density and volume heat generation rates.
2. Thermal flux density is applied in the first seconds (*beam diameter/laser transverse speed*) with the maximum energy intensity value of the corresponding Gaussian beam.
3. Volume heat generation rate is applied in the rest of the time within each track or each layer with an average value calculated by absorbed energy divided by the deposited volume.

The finite element model was implemented by solving the following heat transfer equations. The governing equation of 3D heat transfer is given in (1):

$$\nabla \cdot k \nabla T + \dot{q} = \rho c_p \frac{\partial T}{\partial t}, \quad (1)$$

where  $T$  is temperature,  $t$  is time,  $C_p$  is specific heat at constant pressure,  $\rho$  is density,  $k$  is thermal conductivity, and  $\nabla$  is the Hamilton operator which is equal to  $(\frac{\partial}{\partial x}, \frac{\partial}{\partial y}, \frac{\partial}{\partial z})$ . There was no internal heat generation, so the  $\dot{q}$  was set to zero. Density, thermal conductivity, and specific heat were all implemented as temperature-dependent parameters. Latent heat effects were modeled using (2) [8].

$$c_p^*(T) = c_p(T) + \frac{L}{T_m - T_0}, \quad (2)$$

where  $c_p^*(T)$  is the modified specific heat,  $c_p(T)$  is the temperature-dependent specific heat,  $L$  is the latent heat of fusion,  $T_m$  is the melting temperature, and  $T_0$  is the ambient temperature. The temperature-dependent property values of the Ti-6Al-4V substrate and deposit were taken from [9].

Fixtures play an important role as heat sinks in the laser deposition process [5]. In the current model, two bolts were simplified as two blocks at two ends of the substrate, and the base plate underneath the substrate was also modeled as a block, as shown in Fig. 2 (a), where their material properties were assigned using the equivalent mass method as proposed in [5]; mass, thermal conductivity, and specific heat were kept the same, but density was modified according to the modeled fixture volume. As shown in Fig. 2 (a), the model was meshed with a non-uniform distributed element size and only used fine mesh at volumes of interest to reduce the model size and computational time. The final model contains total 14922 elements and 17150 nodes.

The initial condition for the numerical simulation domain was set to a uniform temperature field equal to ambient temperature (300 K), which is defined as shown in (3).

$$T|_{t=0} = T_0, \quad 0 \leq x \leq L_1, \quad 0 \leq y \leq L_2, \quad 0 \leq z \leq L_3 \quad (3)$$

The boundary conditions for all surfaces (both substrate and deposit) were set to have convection and radiation losses (4) [7]:

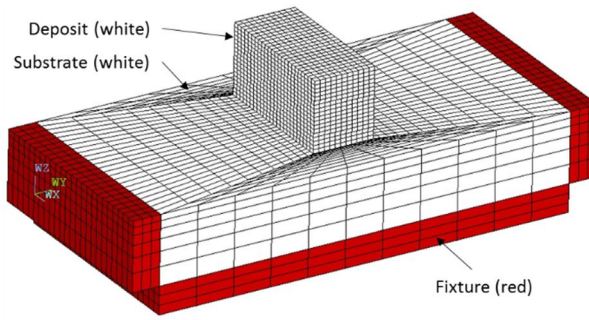
$$k(\nabla T \cdot \vec{n})|_{\Omega} = h(T - T_a)|_{\Omega} + \varepsilon\sigma(T^4 - T_e^4)|_{\Omega} - Q_r|_{\Omega_{Laser}}, \quad (4)$$

where  $h$  was convective heat transfer coefficient,  $T_a$  was the ambient temperature,  $\varepsilon$  was emission coefficient,  $\sigma$  was the Stefan-Boltzmann constant ( $5.67 \times 10^{-8} \text{ W/m}^2 \text{ K}^4$ ),  $T_e$  was the wall temperature of the sealed chamber and set equal to  $T_a$ , and  $Q_r$  the is the heat input from the laser beam. As new elements changed from death to birth status, the outer surfaces related to boundary conditions were updated.

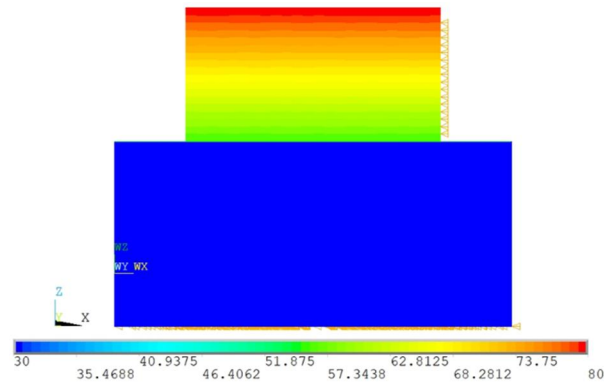
In this case, forced convection needs to be considered as reported in [10], where the decrease of  $h$  as the distance from the top edge of the wall increases was assumed to be linear as provided in (5):

$$h = -1.4z + 80, \quad (5)$$

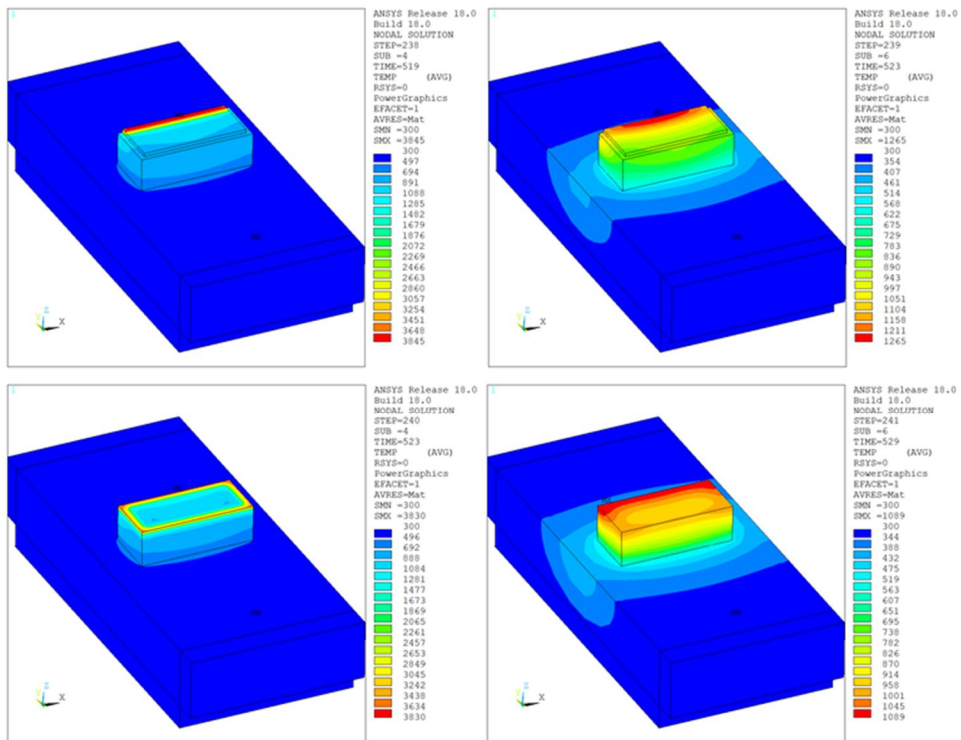
where  $z$  is the distance from the top edge of the wall to the point of interest. The convective heat transfer coefficient distribution at the last step is shown in Fig. 2 (b), where the substrate and fixture were set to free convection when  $z$  was beyond the deposit height and the convective heat transfer coefficient was equal to  $30 \text{ W/m}^2/\text{°C}$ .



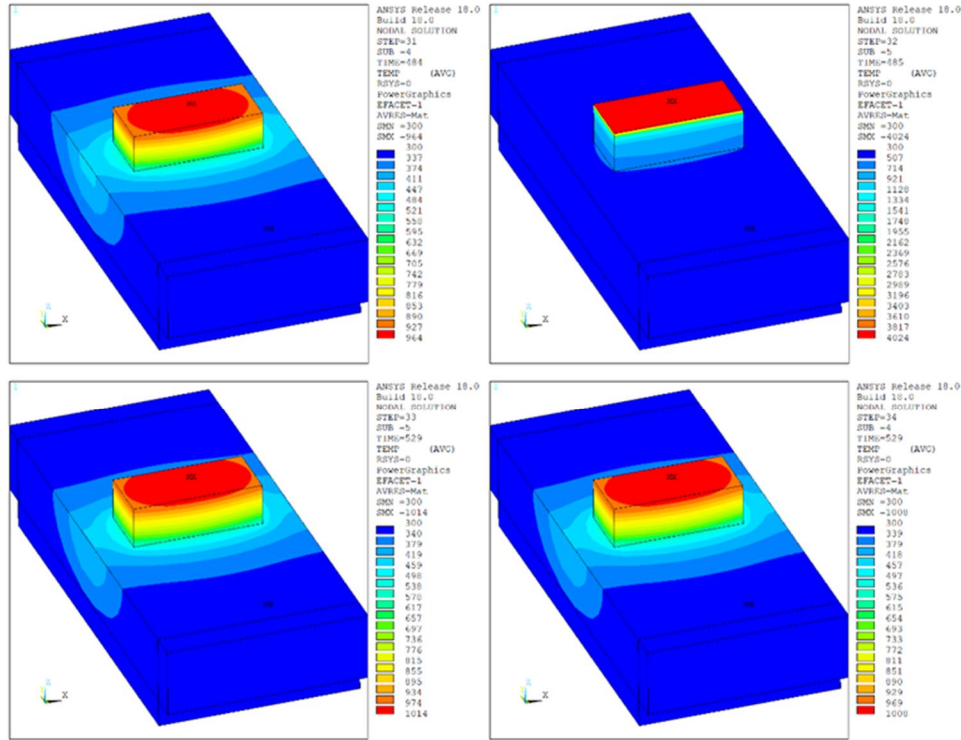
(a)



(b)



(c)



(d)

Fig. 2 FEA model set-up. (a) meshed mode with the simplified fixture (red), the substrate (white) and deposit (white), (b) convection coefficient distribution, (c) temperature distribution at 11<sup>th</sup> layer with track heat source, (d) temperature distribution at 11<sup>th</sup> layer with layer heat source.

The finite element model uses a fixed mesh size for all the substrates, deposits, and fixtures during simulation. To simulate the addition of material in the laser deposition process, a method called element birth and death in ANSYS was employed. The element death function was used to deactivate an element by setting its stiffness to zero, while the element birth function was used to activate an element by setting the right stiffness value. At the start of the simulation, the substrate elements were all activated. However, the deposit elements were activated sequentially to simulate material addition. The element birth and death method application in track-heat-source and layer-heat-source are demonstrated in Fig. 2 (c) and 2 (d), respectively. Fig. 2 (c) shows the tracked heat source process where the heat flux was applied to the last track of the 11<sup>th</sup> layer, followed by the volume heat generation rate. The perimeter scan was simulated after the last track was added, following the same heat source application sequence as the last track. In Fig. 2 (d), the layered heat source process is shown, with the only difference from the track-heat-source method being the material was added layer by layer instead of track by track.

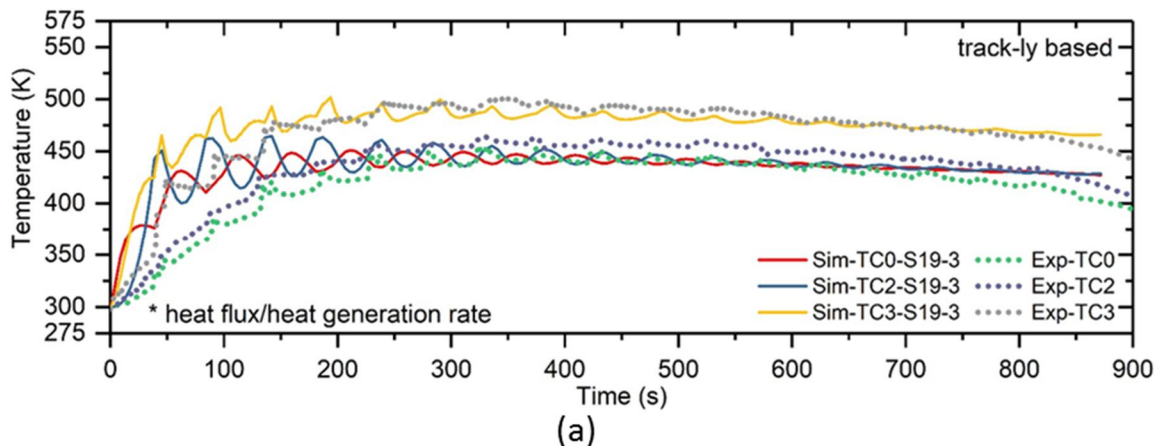
## Results and Discussions

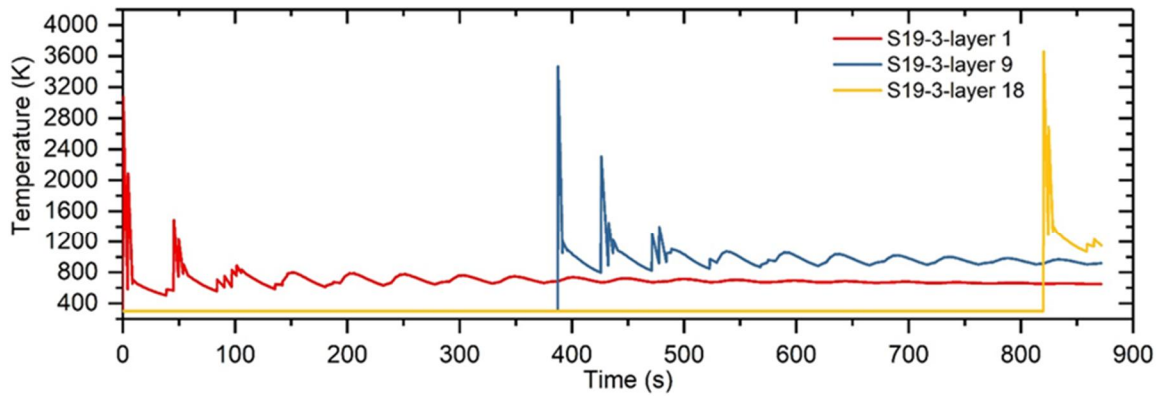
The predicted transient thermal history from the FEA model was validated with the thermocouple data and the comparison results are shown in Fig. 3. TC1 was caught in the laser path during deposition and its measured data was peaked out. Only TC0, TC2, and TC3 measured

data were used in the model validation process. The comparison between TC0, TC2, and TC3 is plotted in Fig. 3 (a), which shows some variance from 0 to approximately 150 seconds and aligns well after that until the end of deposition. The mismatch around 150 seconds is attributed to the difference in loading method in simulation and reality. In simulation, the heat source was applied track by track, but in reality the heat source (laser beam) started from one end and moved to the other end of each track, which led to the locations where the thermocouples were attached to be heated up gradually and reached a peak temperature every time the laser beam passed over. After certain layers, the substrate was heated up and the temperature difference caused by the loading methods was reduced. Heat input and heat loss at evaluated locations on the substrate attained equilibrium for a period of time. As the simulation progressed, equilibrium was broken as heat loss was larger than the heat input, which resulted in a temperature decrease. This phenomenon has been observed in both experimental and simulation data. Based on this validated model, the temperature history of the first track's middle point from the first, ninth, and 18<sup>th</sup> layers were predicted and plotted in Fig. 3 (b), which shows the peak temperature is around 3600 K and close to the evaporation temperature of titanium. The layer heat source method validation results are shown in Fig. 3 (c), where the same trend is captured after about 150 seconds, meaning the simulation and experimental data are well matched. The temperature difference at about 150 seconds also comes from the difference in simulation and experimental loading methods. The predicted middle point peak temperature from the first track of the first, ninth, and 18<sup>th</sup> layers is close to 4200 K using the layer heat source model and exceeds the evaporation temperature of titanium. The peak temperature overestimation comes from the lack of cooling time between each track or layer compared to the real experiments.

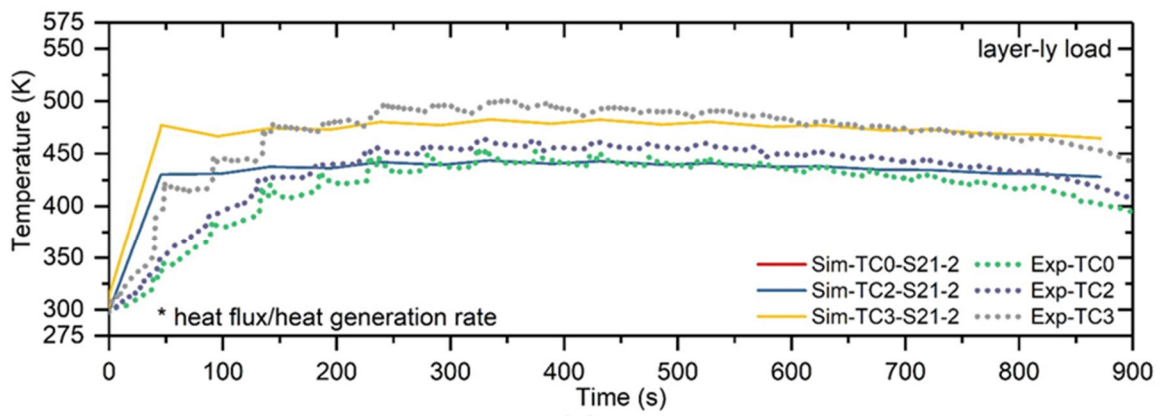
Comparing these two methods, the track-heat-source method has a better resolution than the layer-heat-source method, where the former can capture more thermal details better than the latter method. However, compared to the conventional method which applies the heat source spot by spot, both methods have a lower resolution.

Considering the computational time, the track-heat-source method took about 55 minutes and the layer-heat-source method took about 5 minutes on a computer with an AMD Phenom™ II X6 1090T Processor 3.2 GHz and 16.0 GB RAM hardware. The rougher the prediction model implemented, the less computational time is needed and sacrifices accuracy of the results.

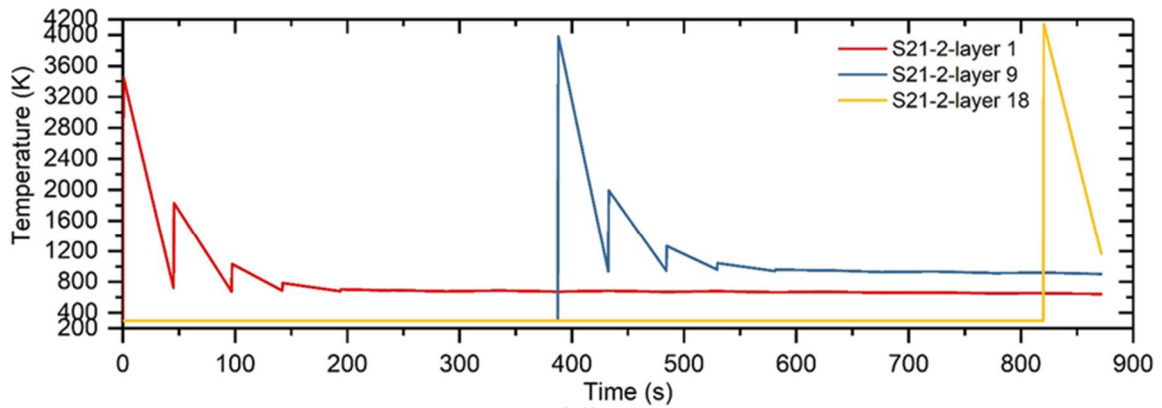




(b)



(c)



(d)

Fig. 3 Model validation results. (a) temperature comparison with track heat source method, (b) prediction of temperature at first, ninth, and 18<sup>th</sup> layers with track heat source method, (c) temperature comparison with layer heat source method, (d) prediction of temperature at first, ninth, and 18<sup>th</sup> layers with layer heat source method.

## **Conclusions**

To conclude, the current work extends the modeling method for fast temperature prediction in large-scale part fabrication using the LMD process. The following are the salient conclusions in the paper:

1. Track- and layer-heat-source methods have the capability for fast temperature prediction in the LMD process.
2. Deposit peak temperature was overestimated in both methods and came from sacrificing modeling details for the computational time-saving purpose.
3. The track-heat-source method has a higher resolution than the layer-heat-source method, but is relatively slower, taking about 11 times longer computational time.

## **Acknowledgments**

This project was supported by The Boeing Company through the Center for Aerospace Manufacturing Technologies (CAMT), National Science Foundation Grants #CMMI-1547042 and CMMI-1625736, and the Intelligent Systems Center (ISC) at Missouri S&T. Their financial support is greatly appreciated.

## **References**

- [1] Costa, L., et al. "Simulation of layer overlap tempering kinetics in steel parts deposited by laser cladding." Proceedings of international conference on metal powder deposition for rapid manufacturing. MPIF, Princeton, NJ, 2002.
- [2] Costa, L., et al. "Rapid tooling by laser powder deposition: process simulation using finite element analysis." *Acta Materialia* 53.14 (2005): 3987-3999.
- [3] Wang, Liang, and Sergio Felicelli. "Process modeling in laser deposition of multilayer SS410 steel." *Journal of Manufacturing Science and Engineering* 129.6 (2007): 1028-1034.
- [4] Crespo, António, and Rui Vilar. "Finite element analysis of the rapid manufacturing of Ti–6Al–4V parts by laser powder deposition." *Scripta Materialia* 63.1 (2010): 140-143.
- [5] Yan, Lei, Yunlu Zhang, and Frank Liou. "A conceptual design of residual stress reduction with multiple shape laser beams in direct laser deposition." *Finite Elements in Analysis and Design* 144 (2018): 30-37.
- [6] Simulia, D. (2011) ABAQUS 6.11 Analysis User's Manual. In. pp. 22-2.
- [7] Yan, Lei, et al. "Simulation of Cooling Rate Effects on Ti–48Al–2Cr–2Nb Crack Formation in Direct Laser Deposition." *JOM* 69.3 (2017): 586-591.
- [8] Toyserkani, Ehsan, Amir Khajepour, and Steve Corbin. "3-D finite element modeling of laser cladding by powder injection: effects of laser pulse shaping on the process." *Optics and Lasers in Engineering* 41.6 (2004): 849-867.

[9] Mills, Kenneth C. Recommended values of thermophysical properties for selected commercial alloys. Woodhead Publishing, 2002.

[10] Heigel, J. C., P. Michaleris, and E. W. Reutzel. "Thermo-mechanical model development and validation of directed energy deposition additive manufacturing of Ti-6Al-4V." Additive manufacturing 5 (2015): 9-19.